Mechanistic Insights into OC–COH Coupling in CO_2 Electroreduction on Fragmented Copper

Kaili Yao[a,b‡], Jun Li[c‡], Haibin Wang[a‡], Ruihu Lu[d], Xiaotao Yang[e], Mingchuan Luo[f], Ning Wang[g], Ziyun Wang[d], Changxu Liu[h,i], Tan Jing[j], Songhua Chen[j], Emiliano Cortés[i], Stefan A. Maier[k,l,i], Sheng Zhang[m], Tieliang Li[n], Yifu Yu[n], Yongchang Liu[o], Xinchen Kang[p], and Hongyan Liang[a*]

[a] School of Materials Science and Engineering and Key Laboratory of Efficient Utilization of Low and Medium Grade Energy, Tianjin University, Tianjin 300350, People's Republic of China

[b] School of Chemical Engineering, Kunming University of Science and Technology, Kunmin 650500, People's Republic of China

[c] Frontiers Science Center for Transformative Molecules, Shanghai Jiao Tong University, Shanghai 200240, People's Republic of China

[d] School of Chemical Sciences, the University of Auckland, Auckland, 1010, New Zealand

[e] School of Mechanical Engineering, Tianjin University, Tianjin 300350, People's Republic of China

[f] Leiden Institute of Chemistry, Leiden University, Einsteinweg 55, 2333 CC Leiden, The Netherlands

[g] Department of Electrical and Computer Engineering, University of Toronto, 35 St George Street, Toronto, Ontario M5S 1A4, Canada

[h] Department of Mathematics, Physics and Electrical Engineering, Northumbria University, Newcastle Upon Tyne NE1 8ST, United Kingdom

[i] Chair in Hybrid Nanosystems, Nanoinstitute Munich, Faculty of Physics, Ludwig Maximilians University of Munich, 80539 Munich, Germany

[j] College of Chemistry and Material Science, Longyan University, Longyan 364012, People's Republic of China

[k] School of Physics and Astronomy, Monash University, Clayton Victoria 3800, Australia

[l] Department of Physics, Imperial College London, London SW7 2AZ, United Kingdom

[m] School of Chemical Engineering and Technology, Tianjin University, Tianjin 300350, People's Republic of China

[n] School of Science, Tianjin University, Tianjin 300350, People's Republic of China

[o] State Key Lab of Hydraulic Engineering Simulation and Safety, School of Materials Science and Engineering, Tianjin University, Tianjin 300354, People's Republic of China

[p] Beijing National Laboratory for Molecular Sciences, Key Laboratory of Colloid and Interface and Thermodynamics, Institute of Chemistry, Chinese Academy of Sciences, Beijing,100190, People's Republic of China

*Email: hongyan.liang@tju.edu.cn

‡K.L.Y., J.L., and H.B.W. contributed equally to this paper.

KEYWORDS. OC−COH coupling, low-coordinated Cu sites, B-doped Cu_2O, fragmented Cu catalysts, carbon dioxide reduction.

ABSTRACT: The carbon-carbon (C−C) bond formation is essential for the electro-conversion of CO_2 into high-energy-density C_{2+} products, and the precise coupling pathways remain controversial. Although recent computational investigations have proposed that the OC−COH coupling pathway is more favorable in specific reaction conditions than the well-known CO dimerization pathway, the experimental evidence is still lacking, partly due to the separated catalyst design and mechanistic/spectroscopic exploration. Here, we employ density functional theory calculations to show that on low-coordinated copper sites, the *CO bindings are strengthened, and the adsorbed *CO coupling with their hydrogenation species, *COH, receives precedence over CO dimerization. Experimentally, we construct a fragmented Cu catalyst with abundant low-coordinated sites, exhibiting a 77.8% Faradaic efficiency for C_{2+} products at 300 mA cm^{-2}. With a suite of *in-situ* spectroscopic studies, we capture an *OCCOH intermediate on the fragmented Cu surfaces, providing direct evidence to support the OC−COH coupling pathway. The mechanistic insights of this research elucidate how to design materials in favor of OC−COH coupling towards efficient C_{2+} production from CO_2 reduction.

The electrocatalytic CO_2 reduction (CO_2R) powered by renewable electricity offers great potential for the scalable utilization of CO_2 to achieve carbon neutrality and storage of intermittent energy.[1-2] Recently, significant efforts have been made to produce multi-carbon (C_{2+}) hydrocarbons and oxygenates, due to their higher value and energy density than mono-carbon (C_1) products.[3-6] For C_{2+} production, the formation of the C−C bond is the rate-determining step, owning to its high energy barrier.[7] It is challenging to identify the dominant C−C coupling pathway given the nature of multiple competitive reactions.[8] The lack of in-depth understanding of the catalytic mechanism exacerbates the difficulty in advancing the catalyst design to promote C_{2+} conversion efficiency.

Previously, the CO dimerization has been suggested as a plausible pathway for C−C bond formation,[9-11], which was also confirmed by online electrochemical mass spectroscopy[12] or by observing *OCCO intermediates via time-resolved attenuated total reflection-surface enhanced infrared absorption spectroscopy (ATR-SEIRAS).[13] However, the discussion about other possible pathways is still open.[14-15] Recently, density functional theory (DFT) calculations suggested the formation of C−C bonds via an OC−COH coupling pathway is thermodynamically and kinetically more favorable than CO dimerized into OCCO.[16-17] When optimizing the Cu−CO interaction on an Au-doped Cu (100)[16] or the CO coverage on Cu (100)[17], the OC−COH coupling can be promoted over the competitive CO dimerization. Moreover, the reaction conditions, such as pH[14] and applied potential[18] also showed effects on C−C coupling selectivity. Despite these extensive theoretical research efforts, the direct observations of the OC−COH coupling remain under-explored, limited by the difficulties in experimental implementation and detection.[19]

To design C_{2+}-producing catalysts, especially for the well-known Cu, the binding energy of *CO is a crucial descriptor allowing control of the desired pathway. Modifying the *CO adsorption on Cu has been reported to enable the optimization of reaction kinetics for OC−COH coupling.[16] Meanwhile, lowering the Cu coordination facilitates *CO adsorption[20] and hydrogenation to COH,[21] which are essential for the OC−COH pathway. Thus, we hypothesize that controlling the *CO adsorption via tuning the coordinated numbers (CNs) of Cu is likely to facilitate the OC−COH coupling.

Here, we present a strategy by introducing low-coordinated Cu sites to enable OC−COH coupling during CO_2R. Computationally, we investigated the adsorption energies of *CO on Cu sites with different CNs. Our results show that low-coordinated Cu sites strengthen *CO adsorption, and facilitate the reduction pathway via *CO hydrogenation to hydroxymethylidyne (*COH) and subsequently coupling with another adsorbed *CO. Experimentally, we prepared a fragmented Cu with abundant low-coordinated sites from the reduction of a boron-doped Cu_2O, as disclosed by *in-situ* X-ray absorption spectroscopy (XAS) and Raman spectroscopy. Using *in-situ* ATR-SEIRAS spectroscopy, we captured the *OCCOH intermediates on the fragmented Cu, validating the OC−COH coupling mechanism. The selective OC−COH coupling endows the fragmented Cu catalysts with a 77.8% Faradaic efficiency (FE) towards C_{2+} products at 300 mA cm^{-2}, which is ~ 30% higher than that of the Cu control.

We first performed density functional theory (DFT) calculations to provide an in-depth understanding of the specific C−C coupling pathways during CO_2R. Given the importance of *CO adsorption in C−C coupling, we thus calculated the adsorption strength of *CO and related key intermediates on the stable Cu (111) slabs[22] with different CNs by introducing vacancies (Figure 1a, Figure S1, and Table S1-S2). Our results demonstrated that both the *CO and *H adsorptions are increased with the decreased CNs, but the enhancement of *CO is greater, resulting in promoted CO_2R rather than HER (Figure S1a).[23-24] The stronger *CO adsorption may lead to the high coverage of *CO, thus decreasing the reaction energies of C−C coupling (Figure S1b-c).[24-25] Besides, the adsorption energy of *COH also increases with the decreased CNs.

We then calculated the transition state barriers of different C−C coupling reactions, OC−CO coupling and OC−COH coupling, as shown in Figures 1b, Figure S2-S4, and Table S3-S8. The results show that the OC−COH coupling becomes more favorable on the low-coordinated Cu sites with CN decreasing from 9 to 6, and their energy barrier is lower than that of the OC−CO pathway.

Taken together, the DFT calculations demonstrated that introducing low-coordinated Cu sites could increase the *CO and *COH binding energies, and lower the energy barrier of C−C bond formation *via* the OC−COH coupling (Figures 1c), promoting the C_{2+} production.

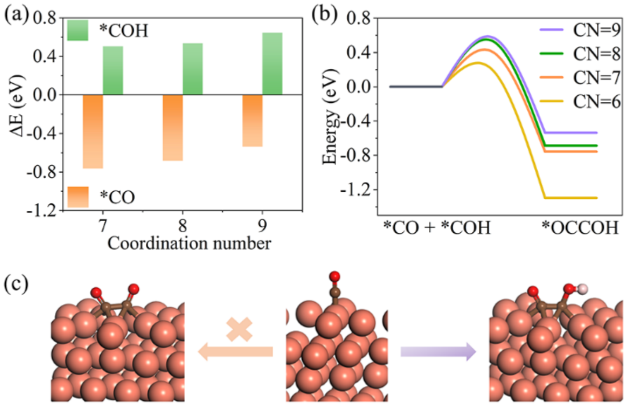

Figure 1. (a) The adsorption energies of *CO and *COH on Cu (111) surface with different CNs. (b) The reaction energies for the OC−COH coupling on the Cu (111) surface with different CNs. (c) Two competitive reaction pathways for C−C coupling. Light brown, copper; pink, hydrogen; red, oxygen; dark brown, carbon.

Experimentally, B-doped copper catalysts were prepared using a wet-chemical approach with sodium borohydride as the reducing agent.[26] As revealed by the X-ray diffraction (XRD), X-ray photoelectron spectroscopy (XPS), scanning electron microscopy (SEM), and transmission electron microscopy (TEM) in Figure 2a and Figure S5-S6, the pristine catalysts showed a particle size of ~ 30 nm, consisting of Cu_2O and B dopants enriched at the surface with a thickness of ~ 2.7 nm,[27] which is denoted as B-doped Cu_2O. The boron contents were determined by the inductively coupled plasma mass spectrometer (ICP-MS), and the averaged atomic ratio of B/Cu is ~ 2.1% as shown in Table S9. During the CO_2R, the catalysts were *in situ* reduced into metallic copper and the nanoparticles were fragmented into flakes with an average size of ~ 6 nm, which were termed fragmented Cu. Size statistics from high-resolution TEM (HRTEM) images are shown in Figures 2b, c, and Figure S7. The B-leaching from the Cu lattice was verified by the high-resolution B 1s XPS (Figure S6f). For comparison, a pure Cu_2O catalyst without B dopants was synthesized. Before CO_2R, the control catalyst showed a similar morphology and size distribution to that of the B-doped Cu_2O (Figure S8). After CO_2R, the control sample evolved into aggregated particles rather than fragments as shown in Figure S9. These results suggested that the boron dopants play a key role in the fragmentation of copper during CO_2R (Figure 2d), as investigated in the following part.

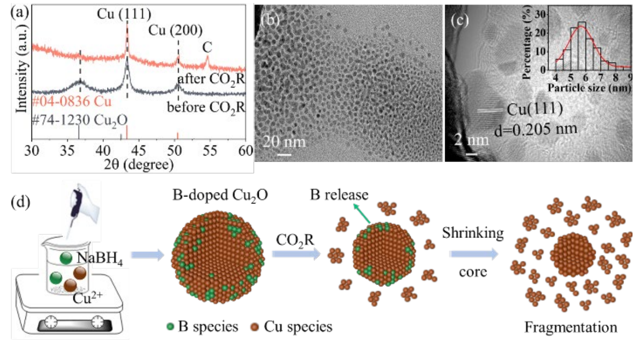

Figure 2. Synthesis and structural characterizations of the catalysts. (a) XRD patterns of B-doped Cu_2O catalysts before and after CO_2R. (b) TEM and (c) HRTEM images of fragmented Cu catalysts after CO_2R. The inset image in (c) is the statistic of particle size. (d) Schematic illustration of the structural evolution of fragmented Cu catalyst.

To understand the fragmentation process of the catalysts, *in-situ* Raman spectroscopy was carried out in the CO_2-saturated 0.1 M $KHCO_3$ electrolyte to monitor the structure evolution (Figure S10). As shown in Figure 3a, both B-doped Cu_2O and control samples showed two peaks at ~ 526 cm^{-1} and 628 cm^{-1} ascribed to Cu_2O[28] under the open circuit potential (OCP), which diminished gradually after applying a negative potential of − 0.7 V *vs* RHE (RHE: reversible hydrogen electrode, Figure S11), indicating a transformation from Cu oxides to metallic Cu. The evolution time of B-doped Cu_2O was ~ 6 min, much longer than that of the control one (2 min), suggesting a retarded reduction of Cu_2O with B dopants. With an increase in reaction time, the Raman signal of adsorbed CO appeared on the fragmented Cu. The C≡O stretching of atop-bound *CO, which is sensitive to the CN of metal atoms,[29] show features on terrace sites at 2050 $\pm$ 10 cm^{-1} and defect sites at 2080 $\pm$ 10 cm^{-1},[30-32] illustrating the existence of imperfect surface.

The catalysts' chemical valence state evolution was monitored by *in-situ* XAS at − 0.7 V *vs* RHE (Figure S12 and Figure S13). The time-dependent Cu *K*-edge X-ray absorption near-edge spectra (XANES) of B-doped catalysts showed that the pristine phase was Cu_2O, which transformed into Cu in ~ 5 min, and then kept stable (Figure 3b-d, Figure S14, Table S10). By performing Fourier transform of the extended X-ray absorption fine structure (EXAFS), we found that a standard Cu-Cu bond with a distance of 2.54 Å and a CN of 3.9 emerged at 90 s (Figure 3e, Figure S15, Table S11). With an increased reaction time, the CN increased and was stabilized at 8.9 $\pm$ 0.5 (Figure 3f, Table S11), and no longer change was observed when further increasing the reduction time, confirming the stability of the low-coordinated Cu atom (Figure S16, Table S12). The low CN of fragmented Cu, compared to a CN of 12 of full coordinated Cu bulk, indicated the presence of imperfect surfaces, such as defects or vacancies,[33] consistent with our *in-situ* Raman results. Moreover, time-dependent XAS were also performed at different applied potentials as shown in Figure S17. The results showed that the increased negative potential led to a faster Cu_2O reduction but with a similar CN of ~ 9 for the derived fragmented Cu (Figure S18 and Table S13).

Taken together, we propose that the B-dopant assists the fragmentation of copper catalysts. It was reported that boron binds strongly with Cu on the sub-surface than on the surface,[34] which might retard the B migration[35-37] and Cu_2O reduction under negative potentials. The slow evolution from the B-doped pre-catalysts to metallic Cu catalysts and the continuing migration of B species out of Cu induce the collapse of original structures, resulting in the formation of fragments with abundant surface vacancies or defects.

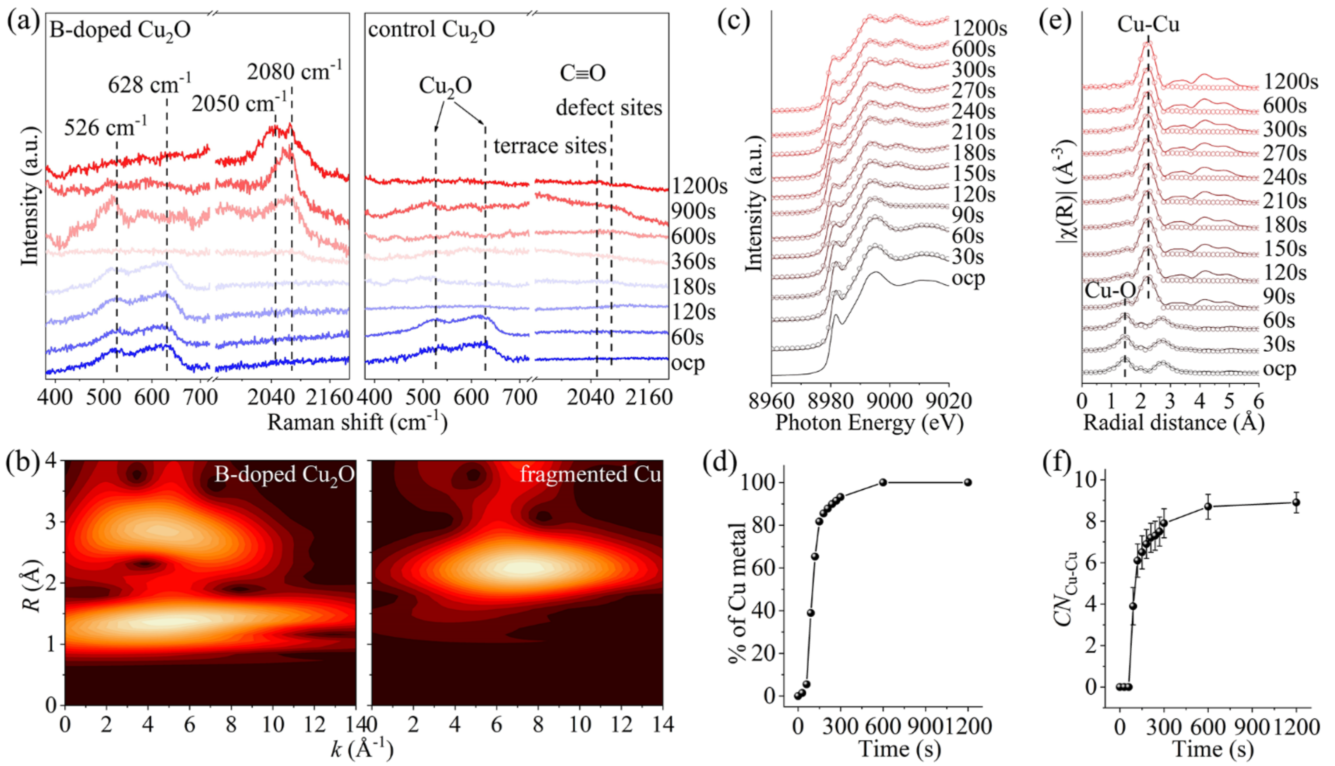

Figure 3. *In-situ* spectra for catalysts' evolution. (a) Time-dependent *in-situ* Raman spectroscopy for B-doped Cu_2O and control sample. (b) Wavelet transform of Cu *K*-edge for B-doped Cu_2O and fragmented Cu. (c-f) Time-dependent *in-situ* XAS measurements for B-doped Cu_2O: Cu K-edge XANES spectra overlapped with linear combination fitting spectra (c) and the corresponding fitted metallic Cu percentage (d); experimental and fitted EXAFS spectra in R space (e), and fitted CN of the first intermetallic Cu−Cu shell (f). In (c) and (e), solid lines represent the experiment data and circles represent the fitting spectra. All measurements were performed at −0.7 V *vs* RHE in 0.1 M $KHCO_3$.

Electrocatalytic CO_2R of two samples was performed in a flow-cell system (Figure 4a and Figure S19). Fragmented Cu reached a FE_{C2+} of 77.8% at a current density of 300 mA cm^{-2} at − 0.69 V *vs* RHE, which is ~ 30% higher than that of the control Cu (Figure 4b, c, and Figure S20 − S23). Also, the FE_{H2} on the fragmented Cu electrode was suppressed to 6.9%, which was much lower than 22.2% of the control Cu (Figure 4b, Table S14 – S17). The CO_2R performance of different catalysts was also evaluated in H-cell using 0.1 M $KHCO_3$ as the electrolyte (Figure S24), and the fragmented Cu outperformed the control Cu.

In-situ Raman spectroscopic techniques deliver direct information regarding the key intermediates. As shown in Figure 4d and Figure S25a, on the fragmented Cu electrode, the peaks at 240 − 430 cm^{-1} and 1900 − 2130 cm^{-1}, associated with the Cu−CO rotation and stretch and the C≡O stretch, respectively, appear simultaneously at a low potential of −0.2 V *vs* RHE, indicating that the *CO adsorption takes place.[38-39] Noting that the high-frequency band (HFB) and the low-frequency band (LFB) of linear CO blue-shifted with increased applied potentials, attributing to the electrochemical Stark effect (Figure 4d and Figure S25b).[32, 38] In comparison, the Cu−CO Raman signals on the control sample appear at a higher potential (− 0.5 V *vs* RHE) with a less pronounced peak, implying less accumulation of *CO.[40] Considering the same testing conditions, these results suggest that the *CO generation and adsorption on fragmented Cu are more likely than on the control Cu.

In-situ ATR-SEIRAS detection of the CO_2R intermediates was used to provide direct evidence for identifying the reaction pathway (Figure S26). As shown in Figure 4e and Figure S27, the peak related to the C=O stretching band of the *OCCOH intermediate at 1587 cm^{-1} is evident on the fragmented Cu due to its strong adsorption energy on the low-coordinated Cu sites (Figure S28, Table S18).[41-43] The peak features of different carbonaceous intermediates can be further identified by DFT calculations, and the C=O stretching vibrations of CO, OCCO, and OCCOH intermediates are 1680.1 cm^{-1}, 1189.5 cm^{-1}, and 1560.7 cm^{-1}, respectively (Table S19).[19] The peak intensity increases under more negative potentials, consistent with the trend of enhanced C_{2+} formation rates (Figure 4c).[15] However, no peaks located at 1500 – 1700 cm^{-1} are observed on the control sample, and only an individual band near 1405 cm^{-1} related to bidentate COO^- species is detected.[44] Notably, the peaks between 2050 – 2150 cm^{-1} could be assigned to *CO species,[45-46] the peak intensity increases firstly and then decreases, indicating that the high coverage of surface adsorbed *CO is beneficial for generating C_{2+} products,[47] but the fast consumption of *CO via further reaction leads to the decreased intensity of *CO.[48] At the potential of −0.8 V *vs* RHE, the C≡O band located at 2092 cm^{-1} on the fragmented Cu, which red-shifted to 2100 cm^{-1} on the control Cu, indicating a stronger Cu−CO interaction on the fragmented Cu surface.[42] The spectroscopic results evidence that the low-coordinated sites on the fragmented Cu provide a stronger interaction with the *CO species, and then promote the C−C coupling through the OC−COH pathway, consistent with the DFT results.

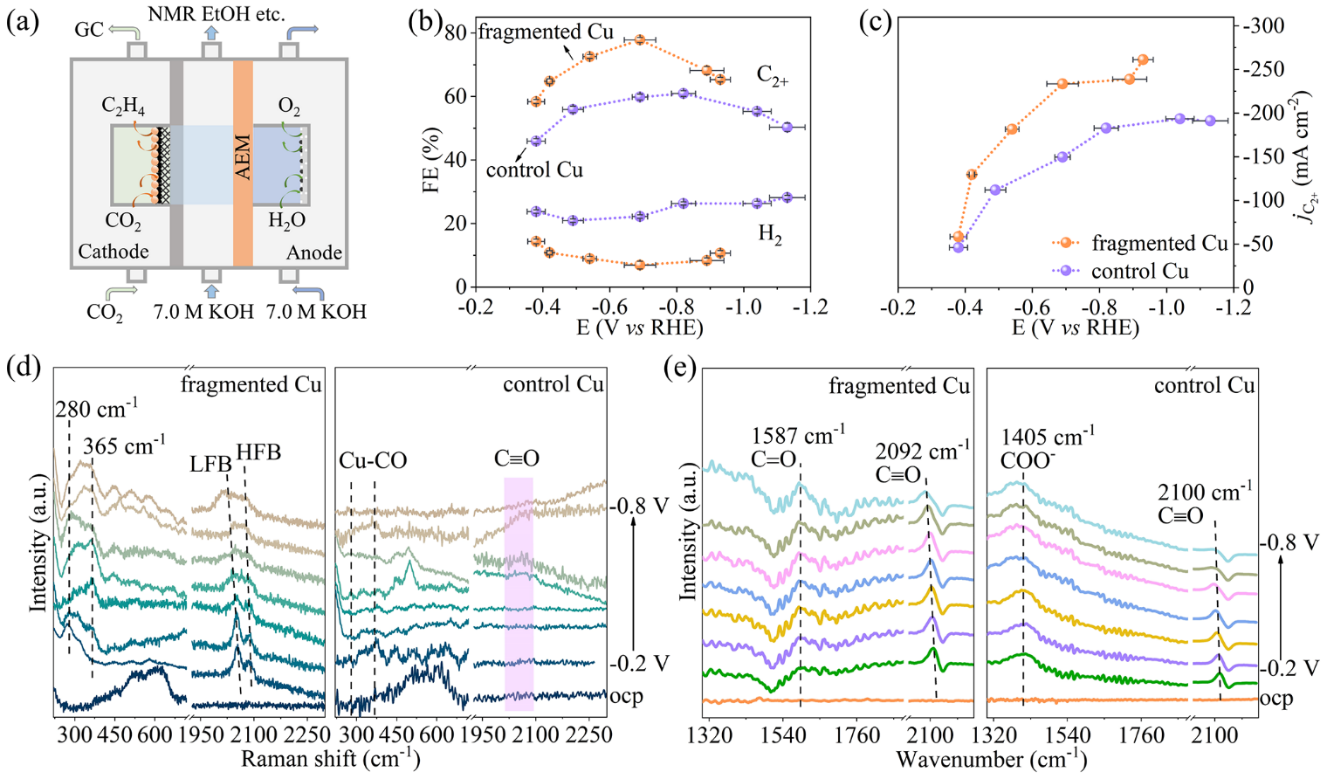

Figure 4. Electrocatalytic performance and analysis of the reaction pathway. (a) Schematic diagram of the flow-cell system with the gas diffusion layer. (b) FEs of C_{2+} and HER, and (c) partial current density of C_{2+} products of fragmented Cu and control Cu catalyst in 7.0 M KOH at various potentials. (d) *In-situ* Raman spectra and (e) *In-situ* ATR-SEIRAS of fragmented Cu and control sample, which were performed during CO_2R at various potentials in CO_2-saturated 0.1 M $KHCO_3$.

In summary, we developed a class of fragmented Cu catalysts to accelerate OC−COH coupling towards enhanced C_{2+} productions from CO_2R. The fragmented Cu catalysts, derived from B-doped Cu_2O, show a 77.8% FE_{C2+} at a current density of 300 mA cm^{-2}, 30% higher than that of the control Cu. DFT calculations and *in-situ* spectroscopies suggested that the low-coordinated Cu active sites on fragmented Cu favor the OC−COH coupling pathway, contributing to the enhanced C_{2+} selectivity.

ASSOCIATED CONTENT

Supporting Information

The Supporting Information is available free of charge via the Internet at http://pubs.acs.org/doi/××.

Experimental, characterizations, and theoretical calculations details, figures of SEM images, XRD patterns, XPS spectra, HRTEM images, XANES and EXAFS spectra, FFT patterns, the photograph of the electrochemical cell for *in-situ* Raman measurements and ATR-SEIRAS measurements, flow-cell reactor, schematic illustration of the *in-situ* XAS measurements, products selectivity and current density, tables of the calculation results, parameters, and selectivities.

Notes

The authors declare no competing financial interest.

ACKNOWLEDGMENT

This work was supported by the National Natural Science Foundation of China (NSFC No. 51771132), the Program for Young and Middle-aged Teachers in Science Research of Fujian Province (No. JAT210433), and the open fund project of Qinghai Minzu University - Nanomaterials and Nanotechnology Team & Platform (2021GFW-0888). We also acknowledge funding and support from the Deutsche Forschungsgemeinschaft (DFG, German Research Foundation) under Germany´s Excellence Strategy – EXC 2089/1 – 390776260, the Bavarian program Solar Energies Go Hybrid (SolTech), the Center for NanoScience (CeNS) and the European Commission through the ERC Starting Grant CATALIGHT (802989). We acknowledge the Paul Scherrer Institut, Villigen, Switzerland, for the provision of synchrotron radiation beamtime at the beamline SuperXAS of the SLS and would like to thank M. Nachtegaal for the assistance. The computational study is supported by the Marsden Fund Council from Government funding and managed by the Royal Society Te Apārangi. ZW and RL wish to acknowledge the use of New Zealand eScience Infrastructure (NeSI) high-performance computing facilities, consulting support, and/or training services as part of this research. S.A.M. additionally acknowledges the EPSRC (EP/W017075/1) and the Lee-Lucas Chair in Physics.

REFERENCES

(1) Ma, W.; He, X.; Wang, W.; Xie, S.; Zhang, Q.; Wang, Y., Electrocatalytic Reduction of CO_2 and CO to Multi-

Carbon Compounds over Cu-Based Catalysts. *Chem. Soc. Rev.* **2021,** *50* (23), 12897-12914.
(2) Zhu, S.; Delmo, E. P.; Li, T.; Qin, X.; Tian, J.; Zhang, L.; Shao, M., Recent Advances in Catalyst Structure and Composition Engineering Strategies for Regulating CO_2 Electrochemical Reduction. *Adv. Mater.* **2021,** *33* (50), 2005484.
(3) Wang, H.; Tzeng, Y. K.; Ji, Y.; Li, Y.; Li, J.; Zheng, X.; Yang, A.; Liu, Y.; Gong, Y.; Cai, L.; Li, Y.; Zhang, X.; Chen, W.; Liu, B.; Lu, H.; Melosh, N. A.; Shen, Z. X.; Chan, K.; Tan, T.; Chu, S.; Cui, Y., Synergistic Enhancement of Electrocatalytic CO_2 Reduction to C_2 Oxygenates at Nitrogen-Doped Nanodiamonds/Cu Interface. *Nat. Nanotechnol.* **2020,** *15* (2), 131-137.
(4) Kim, J. Y.; Hong, D.; Lee, J. C.; Kim, H. G.; Lee, S.; Shin, S.; Kim, B.; Lee, H.; Kim, M.; Oh, J.; Lee, G. D.; Nam, D. H.; Joo, Y. C., Quasi-Graphitic Carbon Shell-Induced Cu Confinement Promotes Electrocatalytic CO_2 Reduction toward C_{2+} Products. *Nat. Commun.* **2021,** *12* (1), 3765.
(5) Fan, L.; Xia, C.; Yang, F.; Wang, J.; Wang, H.; Lu, Y., Strategies in Catalysts and Electrolyzer Design for Electrochemical CO_2 Reduction toward C_{2+} Products. *Sci. Adv.* **2020,** *6* (8), 3111.
(6) Yao, K.; Xia, Y.; Li, J.; Wang, N.; Han, J.; Gao, C.; Han, M.; Shen, G.; Liu, Y.; Seifitokaldani, A.; Sun, X.; Liang, H., Metal-Organic Framework Derived Copper Catalysts for CO_2 to Ethylene Conversion. *J. Mater. Chem. A* **2020,** *8* (22), 11117-11123.
(7) Zhong, D.; Zhao, Z. J.; Zhao, Q.; Cheng, D.; Liu, B.; Zhang, G.; Deng, W.; Dong, H.; Zhang, L.; Li, J.; Li, J.; Gong, J., Coupling of Cu(100) and (110) Facets Promotes Carbon Dioxide Conversion to Hydrocarbons and Alcohols. *Angew. Chem., Int. Ed.* **2021,** *60* (9), 4879-4885.
(8) Zheng, Y.; Vasileff, A.; Zhou, X.; Jiao, Y.; Jaroniec, M.; Qiao, S.-Z., Understanding the Roadmap for Electrochemical Reduction of CO_2 to Multi-Carbon Oxygenates and Hydrocarbons on Copper-Based Catalysts. *J. Am. Chem. Soc.* **2019,** *141* (19), 7646-7659.
(9) Sandberg, R. B.; Montoya, J. H.; Chan, K.; Norskov, J. K., CO-CO Coupling on Cu Facets: Coverage, Strain and Field Effects. *Surf. Sci.* **2016,** *654*, 56-62.
(10) Montoya, J. H.; Shi, C.; Chan, K.; Nørskov, J. K., Theoretical Insights into a CO Dimerization Mechanism in CO_2 Electroreduction. *The Journal of Physical Chemistry Letters* **2015,** *6* (11), 2032-2037.
(11) Wu, Z. Z.; Zhang, X. L.; Niu, Z. Z.; Gao, F. Y.; Yang, P. P.; Chi, L. P.; Shi, L.; Wei, W. S.; Liu, R.; Chen, Z.; Hu, S.; Zheng, X.; Gao, M. R., Identification of Cu(100)/Cu(111) Interfaces as Superior Active Sites for CO Dimerization During CO_2 Electroreduction. *J. Am. Chem. Soc.* **2022,** *144* (1), 259-269.
(12) Schouten, K.; Kwon, Y.; Van der Ham, C.; Qin, Z.; Koper, M., A New Mechanism for the Selectivity to C_1 and C_2 Species in the Electrochemical Reduction of Carbon Dioxide on Copper Electrodes. *Chem. Sci.* **2011,** *2* (10), 1902-1909.
(13) Kim, Y.; Park, S.; Shin, S. J.; Choi, W.; Min, B. K.; Kim, H.; Kim, W.; Hwang, Y. J., Time-Resolved Observation of C-C Coupling Intermediates on Cu Electrodes for Selective Electrochemical CO_2 Reduction. *Energy Environ. Sci.* **2020,** *13* (11), 4301-4311.
(14) Xiao, H.; Cheng, T.; Goddard, W. A.; Sundararaman, R., Mechanistic Explanation of the pH Dependence and Onset Potentials for Hydrocarbon Products from Electrochemical Reduction of CO on Cu (111). *J. Am. Chem. Soc.* **2016,** *138* (2), 483-486.
(15) Ma, W.; Xie, S.; Liu, T.; Fan, Q.; Ye, J.; Sun, F.; Jiang, Z.; Zhang, Q.; Cheng, J.; Wang, Y., Electrocatalytic Reduction of CO_2 to Ethylene and Ethanol Through Hydrogen-Assisted C-C Coupling over Fluorine-Modified Copper. *Nat. Catal.* **2020,** *3* (6), 478-487.
(16) Zhi, X.; Jiao, Y.; Zheng, Y.; Qiao, S. Z., Key to C_2 Production: Selective C-C Coupling for Electrochemical CO_2 Reduction on Copper Alloy Surfaces. *Chem. Commun.* **2021,** *57* (75), 9526-9529.
(17) Ou, L.; He, Z., Mechanism for CO_2 Electroreduction into C_2 Products at the Low Overpotential: Theoretical Insights from an Improved Electrode/Solution Interface Model. *Surf. Sci.* **2021,** *705*, 121782.
(18) Luo, W.; Nie, X.; Janik, M. J.; Asthagiri, A., Facet Dependence of CO_2 Reduction Paths on Cu Electrodes. *ACS Catalysis* **2016,** *6* (1), 219-229.
(19) Perez-Gallent, E.; Figueiredo, M. C.; Calle-Vallejo, F.; Koper, M. T. M., Spectroscopic Observation of a Hydrogenated CO Dimer Intermediate during CO Reduction on Cu(100) Electrodes. *Angew. Chem., Int. Ed.* **2017,** *56* (13), 3621-3624.
(20) Li, J.; Che, F.; Pang, Y.; Zou, C.; Howe, J. Y.; Burdyny, T.; Edwards, J. P.; Wang, Y.; Li, F.; Wang, Z.; De Luna, P.; Cao-Thang, D.; Zhuang, T.-T.; Saidaminov, M. I.; Cheng, S.; Wu, T.; Finfrock, Y. Z.; Ma, L.; Hsieh, S.-H.; Liu, Y.-S.; Botton, G. A.; Pong, W.-F.; Du, X.; Guo, J.; Sham, T.-K.; Sargent, E. H.; Sinton, D., Copper Adparticle Enabled Selective Electrosynthesis of n-Propanol. *Nat. Commun.* **2018,** *9*, 4614.
(21) Xu, Y.; Li, F.; Xu, A.; Edwards, J. P.; Hung, S.-F.; Gabardo, C. M.; O'Brien, C. P.; Liu, S.; Wang, X.; Li, Y.; Wicks, J.; Miao, R. K.; Liu, Y.; Li, J.; Huang, J. E.; Abed, J.; Wang, Y.; Sargent, E. H.; Sinton, D., Low Coordination Number Copper Catalysts for Electrochemical CO_2 Methanation in a Membrane Electrode Assembly. *Nat. Commun.* **2021,** *12* (1), 2932-2932.
(22) Wang, Y.; Wang, Z.; Dinh, C.-T.; Li, J.; Ozden, A.; Golam Kibria, M.; Seifitokaldani, A.; Tan, C.-S.; Gabardo, C. M.; Luo, M.; Zhou, H.; Li, F.; Lum, Y.; McCallum, C.; Xu, Y.; Liu, M.; Proppe, A.; Johnston, A.; Todorovic, P.; Zhuang, T.-T.; Sinton, D.; Kelley, S. O.; Sargent, E. H., Catalyst Synthesis under CO_2 Electroreduction Favours Faceting and Promotes Renewable Fuels Electrosynthesis. *Nat. Catal.* **2020,** *3* (2), 98-106.
(23) Ji, Y.; Chen, Z.; Wei, R.; Yang, C.; Wang, Y.; Xu, J.; Zhang, H.; Guan, A.; Chen, J.; Sham, T.-K.; Luo, J.; Yang, Y.; Xu, X.; Zheng, G., Selective CO-to-Acetate Electroreduction via Intermediate Adsorption tuning on Ordered Cu–Pd Sites. *Nat. Catal.* **2022,** *5* (4), 251-258.
(24) Li, X.; Liu, Q.; Wang, J.; Meng, D.; Shu, Y.; Lv, X.; Zhao, B.; Yang, H.; Cheng, T.; Gao, Q.; Li, L.; Wu, H. B., Enhanced Electroreduction of CO_2 to C_{2+} Products on Heterostructured Cu/oxide Electrodes. *Chem* **2022,** *8*, 1-15.

(25) Kong, X.; Zhao, J.; Ke, J.; Wang, C.; Li, S.; Si, R.; Liu, B.; Zeng, J.; Geng, Z., Understanding the Effect of *CO Coverage on C–C Coupling toward CO_2 Electroreduction. *Nano Lett.* **2022,** *22* (9), 3801–3808.

(26) Carenco, S.; Portehault, D.; Boissiere, C.; Mezailles, N.; Sanchez, C., Nanoscaled Metal Borides and Phosphides: Recent Developments and Perspectives. *Chem. Rev.* **2013,** *113* (10), 7981-8065.

(27) Chen, P. Z.; Xu, K.; Zhou, T. P.; Tong, Y.; Wu, J. C.; Cheng, H.; Lu, X. L.; Ding, H.; Wu, C. Z.; Xie, Y., Strong-Coupled Cobalt Borate Nanosheets/Graphene Hybrid as Electrocatalyst for Water Oxidation under Both Alkaline and Neutral Conditions. *Angew. Chem., Int. Ed.* **2016,** *55* (7), 2488-2492.

(28) Yang, P. P.; Zhang, X. L.; Gao, F. Y.; Zheng, Y. R.; Niu, Z. Z.; Yu, X.; Liu, R.; Wu, Z. Z.; Qin, S.; Chi, L. P.; Duan, Y.; Ma, T.; Zheng, X. S.; Zhu, J. F.; Wang, H. J.; Gao, M. R.; Yu, S. H., Protecting Copper Oxidation State via Intermediate Confinement for Selective CO_2 Electroreduction to C_{2+} Fuels. *J. Am. Chem. Soc.* **2020,** *142* (13), 6400-6408.

(29) Eren, B.; Liu, Z.; Stacchiola, D.; Somorjai, G. A.; Salmeron, M., Structural Changes of Cu(110) and Cu(110)-(2 x 1)-O Surfaces under Carbon Monoxide in the Torr Pressure Range Studied with Scanning Tunneling Microscopy and Infrared Reflection Absorption Spectroscopy. *J. Phys. Chem. C* **2016,** *120* (15), 8227-8231.

(30) Gunathunge, C. M.; Li, X.; Li, J.; Hicks, R. P.; Ovalle, V. J.; Waegele, M. M., Spectroscopic Observation of Reversible Surface Reconstruction of Copper Electrodes under CO_2 Reduction. *J. Phys. Chem. C* **2017,** *121* (22), 12337-12344.

(31) Gunathunge, C. M.; Li, J.; Li, X.; Hong, J. J.; Waegele, M. M., Revealing the Predominant Surface Facets of Rough Cu Electrodes under Electrochemical Conditions. *ACS Catalysis* **2020,** *10* (12), 6908-6923.

(32) An, H.; Wu, L.; Mandemaker, L. D. B.; Yang, S.; de Ruiter, J.; Wijten, J. H. J.; Janssens, J. C. L.; Hartman, T.; van der Stam, W.; Weckhuysen, B. M., Sub-Second Time-Resolved Surface-Enhanced Raman Spectroscopy Reveals Dynamic CO Intermediates during Electrochemical CO_2 Reduction on Copper. *Angew. Chem., Int. Ed.* **2021,** *60* (30), 16576-16584.

(33) Gong, Q.; Ding, P.; Xu, M.; Zhu, X.; Wang, M.; Deng, J.; Ma, Q.; Han, N.; Zhu, Y.; Lu, J.; Feng, Z.; Li, Y.; Zhou, W.; Li, Y., Structural Defects on Converted Bismuth Oxide Nanotubes Enable Highly Active Electrocatalysis of Carbon Dioxide Reduction. *Nat. Commun.* **2019,** *10*, 2807.

(34) Trinh, Q. T.; Banerjee, A.; Yang, Y. H.; Mushrif, S. H., Sub-Surface Boron-Doped Copper for Methane Activation and Coupling: First-Principles Investigation of the Structure, Activity, and Selectivity of the Catalyst. *J. Phys. Chem. C* **2017,** *121* (2), 1099-1112.

(35) Zhao, S.; Yue, H.; Zhao, Y.; Wang, B.; Geng, Y.; Lv, J.; Wang, S.; Gong, J.; Ma, X., Chemoselective Synthesis of Ethanol via Hydrogenation of Dimethyl Oxalate on Cu/SiO_2: Enhanced Stability with Boron Dopant. *J. Catal.* **2013,** *297*, 142-150.

(36) Zhao, Y.; Zhang, J.; Xie, Y.; Sun, B.; Jiang, J.; Jiang, W.-J.; Xi, S.; Yang, H. Y.; Yan, K.; Wang, S.; Guo, X.; Li, P.; Han, Z.; Lu, X.; Liu, H.; Wang, G., Constructing Atomic Heterometallic Sites in Ultrathin Nickel-Incorporated Cobalt Phosphide Nanosheets via a Boron-Assisted Strategy for Highly Efficient Water Splitting. *Nano Lett.* **2021,** *21* (1), 823-832.

(37) Fan, H.; Huang, X.; Shang, L.; Cao, Y.; Zhao, Y.; Wu, L. Z.; Tung, C. H.; Yin, Y.; Zhang, T., Controllable Synthesis of Ultrathin Transition-Metal Hydroxide Nanosheets and their Extended Composite Nanostructures for Enhanced Catalytic Activity in the Heck Reaction. *Angew. Chem., Int. Ed.* **2016,** *55* (6), 2167-2170.

(38) Chernyshova, I. V.; Somasundaran, P.; Ponnurangam, S., On the Origin of the Elusive First Intermediate of CO_2 Electroreduction. *Proc. Natl. Acad. Sci. U. S. A.* **2018,** *115* (40), E9261-E9270.

(39) Li, F.; Li, Y. C.; Wang, Z.; Li, J.; Nam, D. H.; Lum, Y.; Luo, M.; Wang, X.; Ozden, A.; Hung, S. F.; Chen, B.; Wang, Y.; Wicks, J.; Xu, Y.; Li, Y.; Gabardo, C. M.; Dinh, C. T.; Wang, Y.; Zhuang, T. T.; Sinton, D.; Sargent, E. H., Cooperative CO_2-to-Ethanol Conversion via Enriched Intermediates at Molecule-Metal Catalyst Interfaces. *Nat. Catal.* **2020,** *3* (1), 75-82.

(40) Wang, X.; Wang, Z.; García de Arquer, F. P.; Dinh, C.-T.; Ozden, A.; Li, Y. C.; Nam, D.-H.; Li, J.; Liu, Y.-S.; Wicks, J.; Chen, Z.; Chi, M.; Chen, B.; Wang, Y.; Tam, J.; Howe, J. Y.; Proppe, A.; Todorović, P.; Li, F.; Zhuang, T.-T.; Gabardo, C. M.; Kirmani, A. R.; McCallum, C.; Hung, S.-F.; Lum, Y.; Luo, M.; Min, Y.; Xu, A.; O'Brien, C. P.; Stephen, B.; Sun, B.; Ip, A. H.; Richter, L. J.; Kelley, S. O.; Sinton, D.; Sargent, E. H., Efficient Electrically Powered CO_2-to-Ethanol via Suppression of Deoxygenation. *Nat. Energy* **2020,** *5* (6), 478-486.

(41) Liu, W.; Zhai, P.; Li, A.; Wei, B.; Si, K.; Wei, Y.; Wang, X.; Zhu, G.; Chen, Q.; Gu, X.; Zhang, R.; Zhou, W.; Gong, Y., Electrochemical CO_2 Reduction to Ethylene by Ultrathin CuO Nanoplate Arrays. *Nat. Commun.* **2022,** *13* (1), 1877.

(42) Zhu, S.; Li, T.; Cai, W. B.; Shao, M., CO_2 Electrochemical Reduction As Probed through Infrared Spectroscopy. *ACS Energy Letters* **2019,** *4* (3), 682-689.

(43) Zhao, Z. H.; Zhu, H. L.; Huang, J. R.; Liao, P. Q.; Chen, X. M., Polydopamine Coating of a Metal–Organic Framework with Bi-Copper Sites for Highly Selective Electroreduction of CO_2 to C_{2+} Products. *ACS Catalysis* **2022,** *12*, 7986-7993.

(44) Zhu, S.; Jiang, B.; Cai, W. B.; Shao, M., Direct Observation on Reaction Intermediates and the Role of Bicarbonate Anions in CO_2 Electrochemical Reduction Reaction on Cu Surfaces. *J. Am. Chem. Soc.* **2017,** *139* (44), 15664-15667.

(45) Malkani, A. S.; Dunwell, M.; Xuo, B., Operando Spectroscopic Investigations of Copper and Oxide Derived Copper Catalysts for Electrochemical CO Reduction. *ACS Catalysis* **2019,** *9* (1), 474-478.

(46) Heyes, J.; Dunwell, M.; Xu, B., CO_2 Reduction on Cu at Low Overpotentials with Surface-Enhanced in Situ Spectroscopy. *J. Phys. Chem. C* **2016,** *120* (31), 17334-17341.

(47) Zhang, T.; Bui, J. C.; Li, Z.; Bell, A. T.; Weber, A. Z.; Wu, J., Highly Selective and Productive Reduction of

Carbon Dioxide to Multicarbon Products via in Situ CO Management using Segmented Tandem Electrodes. *Nat. Catal.* **2022,** *5* (3), 202-211.
(48) Katayama, Y.; Nattino, F.; Giordano, L.; Hwang, J.; Rao, R. R.; Andreussi, O.; Marzari, N.; Shao-Horn, Y., An in Situ Surface-Enhanced Infrared Absorption Spectroscopy Study of Electrochemical CO_2 Reduction: Selectivity Dependence on Surface C-Bound and O-Bound Reaction Intermediates. *J. Phys. Chem. C* **2019,** *123* (10), 5951-5963.

TOC Graphic

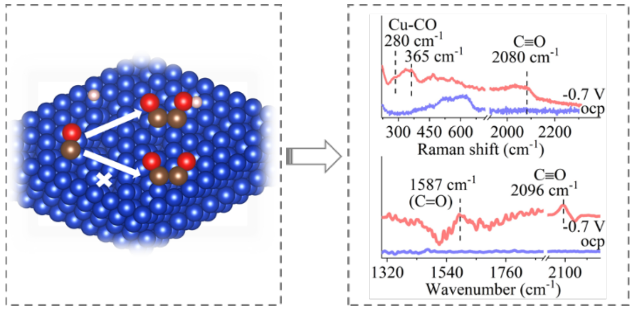

Cu-CO
280 cm-1
365 cm-1
C≡O
2080 cm-1
-0.7 V
ocp
300 450 600 2000 2200
Raman shift (cm-1)
1587 cm-1
(C=O)
C≡O
2096 cm-1
-0.7 V
ocp
1320 1540 1760 2100
Wavenumber (cm-1)